AGU PUBLICATIONS

Tectonics

RESEARCH ARTICLE
10.1002/2016TC004450

Key Points:
- Timing of Neogene Alpine deformation in the Western Alps
- Exhumation of the external crystalline massifs

Supporting Information:
- Supporting Information S1

Correspondence to:
D. Egli,
daniel.egli@geo.unibe.ch

Citation:
Egli, D., N. Mancktelow, and R. Spikings (2017), Constraints from $^{40}Ar/^{39}Ar$ geochronology on the timing of Alpine shear zones in the Mont Blanc-Aiguilles Rouges region of the European Alps, *Tectonics*, *36*, 730–748, doi:10.1002/2016TC004450.

Received 20 DEC 2016
Accepted 3 APR 2017
Accepted article online 6 APR 2017
Published online 27 APR 2017

Constraints from $^{40}Ar/^{39}Ar$ geochronology on the timing of Alpine shear zones in the Mont Blanc-Aiguilles Rouges region of the European Alps

D. Egli[1], N. Mancktelow[2], and R. Spikings[3]

[1]Institute of Geological Sciences, University of Bern, Bern, Switzerland, [2]Department of Earth Sciences, ETH Zürich, Zürich, Switzerland, [3]Department of Earth and Environmental Sciences, University of Geneva, Geneva, Switzerland

Abstract The Mont Blanc and Aiguilles Rouges massifs, which form part of the external crystalline massifs of the western European Alps, record a young and fast exhumation history, as established by an extensive low-temperature thermochronology and geochronology data set. Various kinematic and dynamic models for Oligocene to Neogene deformation and exhumation of the Aiguilles Rouges-Mont Blanc system have been proposed. However, the timing of deformation along major shear zones in and around the massifs, which is crucial to these models, is still controversial. Our new $^{40}Ar/^{39}Ar$ data from key deformation zones in the Mont Blanc area show that NW directed thrusting lasted from Oligocene to mid-Miocene times in the Mont Blanc massif before a NW-ward jump of the deformation front to below the Aiguilles Rouges massif, which led to updoming of the Aiguilles Rouges and Mont Blanc massifs. This deactivated the main NW verging shear zones and caused back-folding and back thrusting east of the Mont Blanc, as well as upward extrusion of the Aiguilles Rouges massif. Subsequently, there was a switch to more coaxial shortening between the Aiguilles Rouges and Mont Blanc massifs associated with strain partitioning and related dextral strike-slip deformation on the eastern side of the Mont Blanc massif.

1. Introduction

Mylonitic and phyllonitic shear zones represent bands of localized deformation developed under ductile or brittle-ductile conditions. In such shear zones, white mica commonly grows synkinematically in a variety of rock types and over a large *P-T* range. Its abundance in low-grade metamorphic rocks provides the potential to directly date deformation by using radiogenic isotope methods, such as $^{40}Ar/^{39}Ar$, K/Ar [*Costa and Maluski*, 1988; *Dunlap et al.*, 1991; *West and Lux*, 1993; *Reddy and Potts*, 1999], and Rb-Sr [e.g., *Müller et al.*, 2000a, 2000b; *Cliff and Meffan-Main*, 2003], as a complement to relative age relationships obtained from field mapping. This study focuses on localized shear zones in and around the Mont Blanc, Mont Chétif, Aiguilles Rouges, and Belledonne basement massifs in the western European Alps (Figure 1). The Mont Blanc massif, as one of the external crystalline massifs, underwent a rapid recent exhumation history, as documented from thermochronology studies [e.g., *Seward and Mancktelow*, 1994; *Bogdanoff et al.*, 2000; *Leloup et al.*, 2005; *Glotzbach et al.*, 2008; *Boutoux et al.*, 2016]. Even though the overall geometry of the Mont Blanc massif is well described [e.g., *Escher et al.*, 1993], the processes leading to its uplift and exhumation and the timing of exhumation and associated deformation are still a matter of debate [e.g., *Leloup et al.*, 2005, 2007; *Rolland et al.*, 2007; *Egli and Mancktelow*, 2013]. The main activity on the major tectonic faults of the area is supposed to have been during the Early- to mid-Miocene, but very recent Late Miocene to Pliocene activity has also been proposed [e.g., *Leloup et al.*, 2005]. This study presents age data from 11 sample locations from six specific areas in the Mont Blanc-Aiguilles Rouges region, representing different stages in the tectonic evolution of the area.

In low-grade shear zones, it is not necessarily straightforward to correlate isotopically determined mineral ages with specific geological processes. The concept of a closure temperature implies that there is effective isotopic closure at a specific temperature (± some uncertainty, typically given as ±50°C) for a particular mineral and isotopic system [*Dodson*, 1973]. However, it has been demonstrated that isotopic diffusion also depends on grain size, cooling rate, intracrystalline deformation, duration of metamorphism, and the availability of hydrous fluids, among the multitude of processes that can affect isotope mobility, and therefore, a closure window defining the partial retention zone of the relevant isotopes is a more appropriate concept [e.g., *Hunziker et al.*, 1992; *Dunlap*, 1997]. Fluid-mineral interaction, deformation, and recrystallization are all processes that may reset isotopic systems at temperatures below their estimated closure temperatures

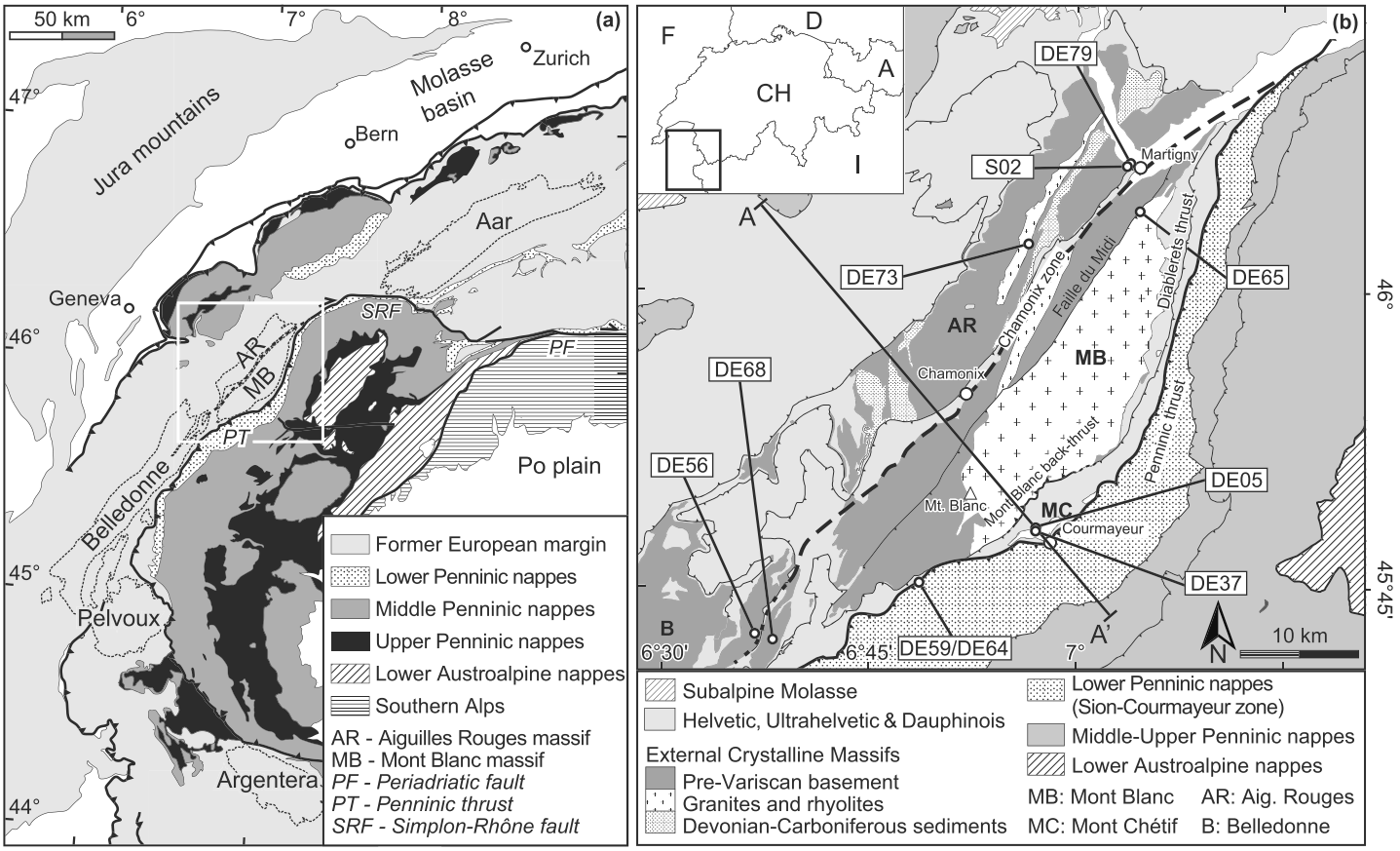

Figure 1. (a) Major paleogeographic units of the Western and central Alps, modified after *Froitzheim et al.* [1996]. The white box shows the location of the study area. (b) Geological setting of the study area indicating the major tectonic units and main tectonic lines, as well as the sample locations. The map is compiled from the tectonic map of Switzerland 1:500000 and Carte géologique de la France 1:250000 (sheet Annecy), modified after *Egli and Mancktelow* [2013].

[e.g., *West and Lux*, 1993; *Dunlap*, 1997; *Villa*, 1998; *Mulch and Cosca*, 2004]. In this case, isotopic age results may reflect the last resetting event or a partial resetting reflecting the influence of the last event or possibly even the summed effect of several preceding events. Independent geological information, such as structural relationships, petrographic and microstructural observations, and the thermal history of rocks are crucial in attempting to understand the significance of sometimes equivocal age spectra and in assigning them to specific metamorphic and/or deformation events. In this study, new $^{40}Ar/^{39}Ar$ ages from individual shear zones potentially related to Neogene exhumation are presented and critically assessed in terms of (1) cooling ages versus recrystallization or neocrystallization and (2) their attribution to distinct periods of tectonic activity in the Mont Blanc-Aiguilles Rouges region. The new data provide important additional time constraints on the activity of major shear zones during the evolution and exhumation of the Mont Blanc and Aiguilles Rouges massifs and, in a broader sense, on the dynamics of the external Alpine collisional wedge in Oligocene to Miocene times.

2. Geological Setting

The Mont Blanc and Aiguilles Rouges massifs constitute part of the external crystalline massifs (ECM) of the European Alps, a series of exposures of pre-Variscan polymetamorphic basement, Late- to post-Variscan intrusions, and Paleozoic sediments, which represent exhumed basement of the former European continental margin [e.g., *von Raumer and Bussy*, 2004] (Figure 1). The study area comprises rocks from the (Ultra-) Helvetic-Dauphinois domain, representing the former European margin and its Mesozoic to Tertiary sedimentary cover, as well as sedimentary successions from the North Penninic Sion-Courmayeur zone of more distal origin, deposited in the Valais trough. Progressive continental collision between Adria and Europe in

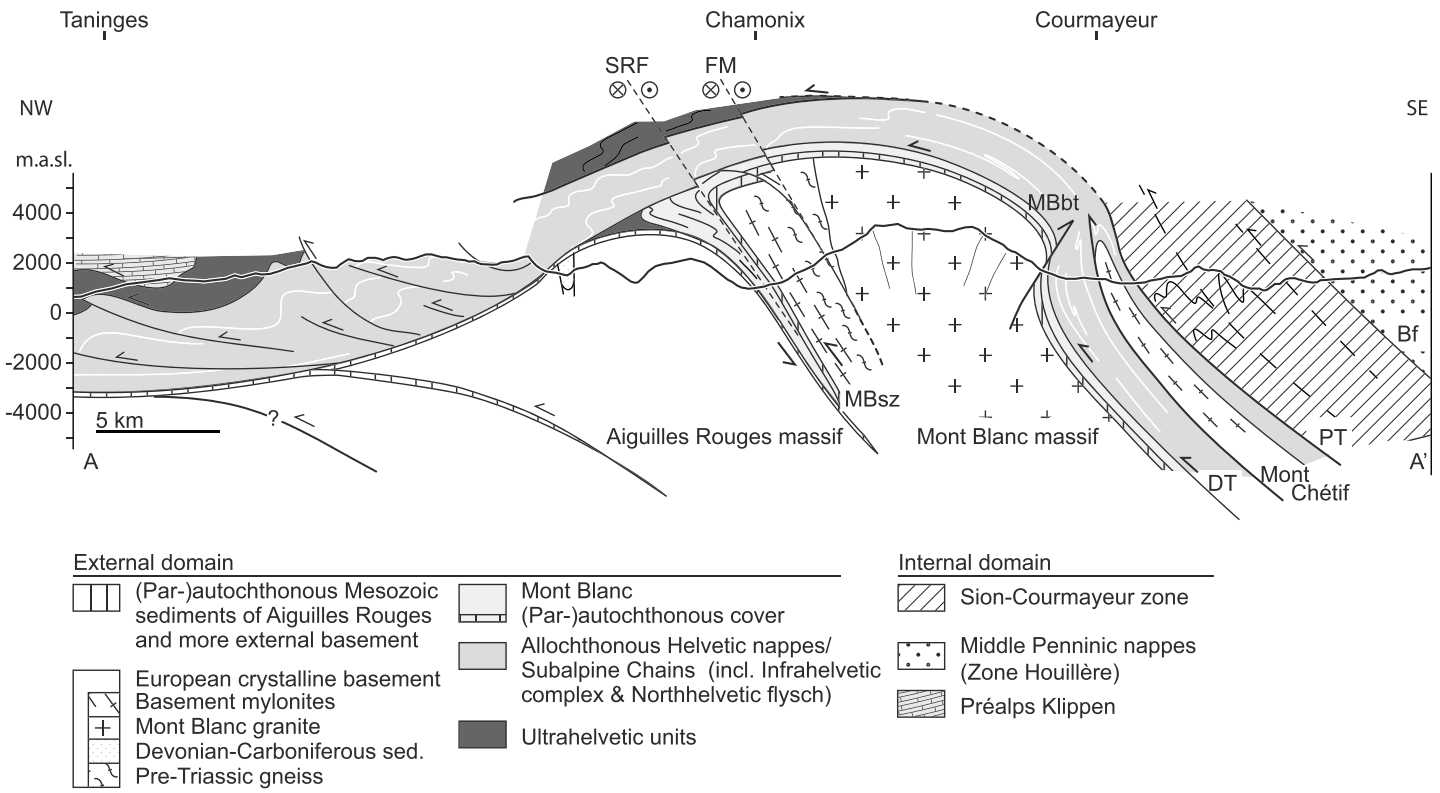

Figure 2. NW-SE section through the southern Mont Blanc and Aiguilles Rouges massifs. Trace of section is given in Figure 1. The section shows the positions of the main fault zones discussed in the text: SRF: Simplon-Rhône fault, FM: Faille du Midi, MBsz: Mont blanc shear zone, MBbt: Mont Blanc back thrust , DT: Diablerets thrust, PT: Penninic thrust, Bf: Briançonnais front. Modified after *Egli and Mancktelow* [2013].

Eocene to Oligocene times caused N to NW directed thrusting and the formation of the Helvetic fold-and-thrust belt [e.g., *Trümpy*, 1980]. Internal folding and thrusting accommodated up to 100 km of shortening [*Masson et al.*, 1980; *Burkhard and Sommaruga*, 1998; *Kempf and Pfiffner*, 2004; *Bellahsen et al.*, 2014]. Continued shortening led to updoming and back-folding of the European basement rocks in Neogene times and resulted in the present-day exposure of the ECM along the outer arc of the Alpine orogen in the footwall of the Penninic thrust [e.g., *Fügenschuh and Schmid*, 2003; *Egli and Mancktelow*, 2013; *Bellahsen et al.*, 2014].

The Mont Blanc basement massif is a SW-NE trending domal culmination that reaches its highest point on the Mont Blanc summit (4808 m) and is framed by major tectonic structures (Figure 2). It is surrounded by Helvetic-Dauphinois Mesozoic (Triassic-Jurassic) sediments with a parautochthonous series directly overlying the basement rocks forming an overturned SE dipping succession on the NW side in the Chamonix valley and an upright sequence along the SE boundary. These parautochthonous metasedimentary successions correspond, at least partly, to the strongly sheared overturned and upright limbs of the Morcles fold-nappe [*Escher et al.*, 1993; *Steck et al.*, 1997]. The shearing of the inverted sequence, extending from the cover units into the basement rocks, is here referred to as the Mont Blanc shear zone (MBsz; Figure 2). Interpreted Late Cenozoic shearing and thrusting of the Mont Blanc basement discordantly over the sedimentary units of the Chamonix valley have been discussed previously in the literature under the same name [*Eltchaninoff-Lancelot et al.*, 1982; *Platt*, 1984; *Leloup et al.*, 2005]. The basal thrust of the Morcles nappe, which is a wide shear zone involving large parts of its overturned limb, is estimated to have a total displacement of 12–20 km during transport of the entire nappe stack over the parautochthonous cover of the Aiguilles Rouges massif [e.g., *Goy-Eggenberger*, 1998; *Kirschner et al.*, 2003]. The (par)autochthonous upright sequence to the SE is separated from the allochthonous Helvetic nappes (here referred to generally as the Diablerets-Wildhorn nappe system) by the Diablerets thrust [e.g., *Crespo-Blanc et al.*, 1995; *Steck et al.*, 2001; *Egli and Mancktelow*, 2013]. The Diablerets-Wildhorn nappe system was completely detached from its basement substratum and sheared over the parautochthonous cover of Mont Blanc along the Diablerets thrust, with an

estimated transport distance of 50–70 km [e.g., *Crespo-Blanc et al.*, 1995; *Kirschner et al.*, 2003; *Kempf and Pfiffner*, 2004]. The contact between the external Helvetic/Ultrahelvetic domain and the more internal Penninic Sion-Courmayeur zone units is marked by the Penninic thrust (PT; Figure 2), which merges with the Rhône fault zone in the Swiss Rhône valley to the north (Figure 1). The dextral transcurrent Rhône fault zone merges to the east with the Miocene low-angle Simplon fault zone, forming the Simplon-Rhône fault system [e.g., *Mancktelow*, 1985; *Steck and Hunziker*, 1994]. Neogene back-folding and back thrusting of the Mont Blanc basement along a NW dipping thrust on its eastern margin in the area of Courmayeur, the Mont Blanc back thrust (MBbt; Figure 2), locally overturned the eastern basement-cover boundary [e.g., *Guermani and Pennacchioni*, 1998; *Steck et al.*, 2001; *Leloup et al.*, 2005; *Rolland et al.*, 2007].

The Alpine metamorphic overprint within the Mont Blanc massif and adjacent areas did not exceed greenschist facies conditions [e.g., *von Raumer*, 1971, 1974; *Aprahamian*, 1988]. Fluid inclusion studies on Alpine fissures in the Mont Blanc massif suggest temperatures of ~400°C and pressures of 2.5–3 kbar (9.5–11 km) during formation of the fissures, which would be in good agreement with the estimated depth of burial of the basement beneath the Helvetic nappe stack [*Poty et al.*, 1974]. $^{40}Ar/^{39}Ar$ step-heating spectra from paragonite-katophorite schists in the NE part of the Mont Blanc massif show well-developed plateau ages between 45.7 and 47.3 Ma, and assuming a closure temperature for paragonite of approximately 300–400°C, Alpine metamorphism could not have exceeded such temperatures after that time [*Marshall et al.*, 1998a, 1998b]. Metamorphism of the frontal parts of the Morcles nappe reached anchizonal to lower greenschist facies conditions, with maximum temperatures around or slightly above 300°C [*Burkhard*, 1988; *Kirschner et al.*, 1995]. However, there is an increase in metamorphic grade toward the sheared limbs in the root zone of the Morcles nappe on either side of the Mont Blanc massif with temperatures exceeding 350°C, as indicated by the transition to stable biotite in the sheared basement of the overturned western boundary [e.g., *Kirschner et al.*, 1995; *Burkhard and Goy-Eggenberger*, 2001; *Egli and Mancktelow*, 2013]. Ductile shear zones in the internal parts of the Mont Blanc basement developed under conditions of 400 ± 25°C and 5 ± 0.5 kbar, with peak metamorphic conditions of 450°C and 4–6 kbar [*Rolland et al.*, 2003; *Rossi et al.*, 2005].

Low-temperature thermochronology studies on the zircon fission track (ZFT), apatite fission track (AFT), and zircon and apatite (U-Th)/He systems (ZHe, AHe) indicate rapid Late Neogene exhumation of the Mont Blanc massif, with published ZFT ages ranging from 11.2 to 15.3 Ma [*Seward and Mancktelow*, 1994; *Glotzbach et al.*, 2011], ZHe ages of 5.8–9.0 Ma [*Boutoux et al.*, 2016], AFT ages of 1.4–7.7 Ma [*Seward and Mancktelow*, 1994; *Leloup et al.*, 2005; *Glotzbach et al.*, 2008], and AHe ages in the range of 1.4–6.4 Ma [*Glotzbach et al.*, 2011]. Raman spectroscopy on carbonaceous material (RSCM) thermometry indicates maximum temperatures in the Aiguilles Rouges cover of about 320°C (±25°C) and 350°C (±25°C) for the Mont Blanc cover, with the thermal peak lasting as long as 5–10 Ma [*Boutoux et al.*, 2016]. The cooling history determined for the northernmost Aiguilles Rouges and Mont Blanc massifs indicates that cooling below 300°C occurred at approximately 20 Ma and that cooling below the AFT closure temperature at around 2.9–4.5 Ma [*Soom*, 1990], with subsequent increased cooling rates potentially related to an increase in topographic relief due to enhanced glacial denudation [*Valla et al.*, 2012].

3. Constraints on the Timing of Alpine Deformation

The timing of Alpine deformation within and around the Mont Blanc basement has been the subject of various studies in recent years and is still a matter of debate [e.g., *Leloup et al.*, 2005, 2007; *Rolland et al.*, 2007, 2008; *Bellahsen et al.*, 2014; *Cenki-Tok et al.*, 2014; *Boutoux et al.*, 2016; *Egli et al.*, 2016]. Onset of deformation in the area postdates movements on the Penninic thrust in Early to Middle Oligocene times [*Ceriani et al.*, 2001; *Simon-Labric et al.*, 2009], with a subsequent complex and heterogeneous deformation history concentrated along major shear zones inside and at the borders of the massif. Allanite ages of 29 ± 1 Ma from the core of the Mont Blanc massif have been interpreted as related to underthrusting of the Mont Blanc massif below the Penninic thrust [*Cenki-Tok et al.*, 2014]. Phengite $^{40}Ar/^{39}Ar$ ages from three locations on the SE flank of the massif yielded consistent ages within error of ~16 Ma, which was interpreted as a deformation age and therefore the time of cessation of SE directed movement along the Mont Blanc back thrust [*Rolland et al.*, 2008]. These mid-Miocene ages correspond to the proposed end of deformation along the NW verging Diablerets thrust [*Crespo-Blanc et al.*, 1995]. Ages from shear-zone-related veins yield similar

Table 1. Sample List, Location, and Results of the $^{40}Ar/^{39}Ar$ White Mica Analyses

Sample	Position (WGS84)	Location	Tectonic Unit	Plateau Age (Ma, 2σ)	Inverse Isochron Age (Ma, 2σ)[a]	Age Gradient (Ma, 2σ)
DE05	45.80118, 6.95367	Mont Chétif	Mont Chétif massif			18.22–20.56
DE37	45.79908, 6.95234	Mont Chétif	Mont Chétif massif	9.56 ± 0.09	8.44 ± 1.27 (0.71)	
DE79	46.10759, 7.06844	La Bâtiaz	Aig. Rouges massif	20.28 ± 0.21	20.18 ± 0.49 (2.19)	
S02	46.10666, 7.06827	La Bâtiaz	Aig. Rouges massif	15.09 ± 0.15	15.07 ± 0.23 (1.83)	
S02 h						10.71–14.63
DE56	45.70559, 6.61956	Beaufort-Roselend	Internal Belledonne massif			13.25–14.97
DE56b				14.54 ± 0.10	14.47 ± 0.33 (2.13)	
DE68	45.70042, 6.63389	Beaufort-Roselend	Internal Belledonne massif		Uninterpretable	
DE65	46.06699, 7.07607	Faille du Midi	Mont Blanc massif			14.30–20.41
DE65b						15.13–20.32
DE59	45.75208, 6.80588	Col de la Seigne	Sion-Courmayeur zone		Uninterpretable	
DE64	45.75182, 6.80593	Col de la Seigne	Sion-Courmayeur zone			27.92–35.20
DE73	46.03954, 6.94168	Vallorcine	Aig. Rouges massif			56.20–79.96

[a]Mean square weighted deviate values.

ages, in the range of 10–16 Ma [*Leutwein et al.*, 1970; *Rossi and Rolland*, 2014]. A biotite $^{40}Ar/^{39}Ar$ age from the same area, presented by *Leloup et al.* [2005], gives a plateau age of 22.8 ± 0.6 Ma and was interpreted to represent the time of cooling below the closure temperature for biotite. On the western flank of the massif, in the NW verging Mont Blanc shear zone, there is a large spread of ages and interpretations are consequently controversial. Most ages from that area are interpreted as cooling ages, with biotite ages from Plan de l'Aiguille of 19.8 Ma [*Rolland et al.*, 2008] and 16.6 ± 0.7 Ma [*Leloup et al.*, 2005]. However, both these ages have disturbed spectra due to excess Ar and these ages probably have to be considered maximum age estimates (detailed argumentation is given in the respective references). Other biotite ages from Plan de l'Aiguille and Aiguille du Midi yielded 63.7 ± 2 Ma and 39.2 ± 1 Ma, respectively, and a K-feldspar age of 16.26 ± 0.01 Ma was also obtained from sheared granite of the Mont Blanc shear zone [*Leloup et al.*, 2005]. Mylonites in the Aiguilles Rouges massif at the border between Switzerland and France at Châtelard are dated to have two deformation ages of 14.3 ± 0.2 and 22.9 ± 0.9 Ma [*Rolland et al.*, 2008]. In this publication the location is incorrectly assigned to the Mont Blanc shear zone and their interpretations therefore differ from ours (see below).

4. Sample Handling and Methodology

Suitable rock samples for $^{40}Ar/^{39}Ar$ dating on white mica were selected by microscopic analysis of thin sections. Samples were fragmented by using the SelFrag® high-voltage pulse power fragmentation machine at ETH Zurich, and white mica separates (~5 mg) were handpicked under a standard binocular microscope, preferably selecting transparent and inclusion-free single crystals or aggregates. The separates were rinsed in deionized water in an ultrasonic bath, packed in copper foil, and irradiated in the Cadmium-Lined in-Core Irradiation Tube (CLICIT) facility of the Training, Research, Isotopes, General Atomics (TRIGA) reactor at Oregon State University for 8 h. Samples were degassed by step-heating with a 55 W CO_2-IR laser (Photon Machines Inc.) that was rastered over the samples to provide even heating of the grains, and the extracted gas was gettered (SAES GP50, ST101, and AP10) in a stainless steel UHV line, after passing through a cold trap chilled to ~150 K. Fish Canyon Tuff sanidine was used as a fluence monitor, with an age of 28.02 ± 0.16 Ma (1σ internal uncertainty [*Renne et al.*, 1998]). Argon isotopes were analyzed at the University of Geneva by using a multicollector GV Instruments Argus mass spectrometer equipped with four high-gain (10^{12} Ω) Faraday detectors and a single 10^{11} Ω Faraday detector (^{40}Ar). Time-zero regressions were fitted to data collected from 12 cycles, and ages were calculated by using the ^{40}K decay constant of *Steiger and Jäger* [1977]. Age plateaus were determined by using the criteria of *Dalrymple and Lanphere* [1974], and data reduction utilized ArArCalc [*Koppers*, 2002].

5. Field Observations and Sample Description

The analyzed samples were collected from key tectonic structures in the Mont Blanc, Mont Chétif, and Aiguilles Rouges basement rocks and its metasedimentary surroundings (Figure 1 and Table 1), and the

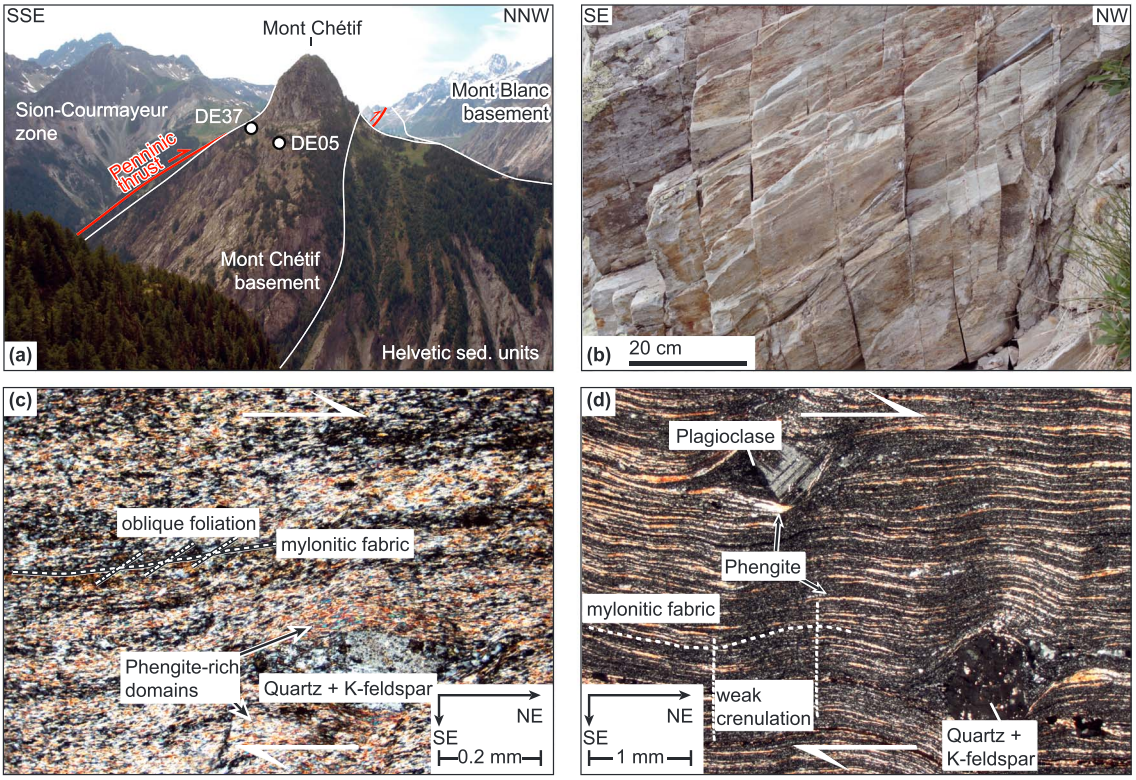

Figure 3. Field observations, sample location, and microphotographs from the Mont Chétif region: (a) Panoramic view of Mont Chétif, seen from Mont de la Saxe. (b) Typical appearance of the phyllonitic rhyolites showing the pervasive main cleavage overprinted by a late steep, spaced, and relatively discrete cleavage (45.80044, 6.95205). (c) Microphotograph of sample DE05 indicating a dextral sense of shear. (d) Microphotograph of sample DE37 with a dextral sense of shear and a weak crenulation overprinting the shear fabric.

respective structures and locations are described in the following. A more extensive description can be found in *Egli* [2013]. Except for samples DE59 and DE64, which were collected from the Sion-Courmayeur zone at Col de la Seigne and are mylonitic metasediments, all samples have quartzo-feldspathic compositions. Major-element mineral analyses and elemental maps were obtained by electron microprobe analysis at ETH Zurich with a JEOL-8200 electron probe. Most white micas have relatively homogeneous phengitic compositions, with the exception of DE68, which shows a muscovite composition.

5.1. Mont Chétif

The Mont Chétif massif (Figure 1), located in the area of Courmayeur in the uppermost Aosta Valley (Italy), forms a 7 km long and few hundred meter wide basement window exposing mainly metagranites and metarhyolites. It is heterogeneously deformed, ranging from effectively undeformed granite, through weakly foliated granites, to mylonites. The Mont Chétif massif is situated southeast of the SE verging oblique reverse-dextral Mont Blanc back thrust and the Diablerets thrust, both of which have been previously interpreted to be active until mid-Miocene times [*Crespo-Blanc et al.*, 1995; *Rolland et al.*, 2008], and within the footwall of the Penninic thrust, which was active during Early to Middle Oligocene [*Ceriani et al.*, 2001; *Simon-Labric et al.*, 2009]. Especially on its southern side, in the immediate footwall of the Penninic thrust, the Mont Chétif massif shows a well-developed mylonitic foliation dipping steeply toward SE, with a stretching lineation plunging shallowly toward ENE and an oblique reverse-dextral or top-to-(west-north-)west sense of shear. This mylonitic foliation is regularly overprinted at a small angle by meter-scale phyllonitic shear zones, reflecting further localization with the same kinematics [*Egli and Mancktelow*, 2013; *Egli et al.*, 2016]. The two analyzed samples DE05 and DE37 were collected from such high-strain zones (Figures 3a and 3b). A weak crenulation overprints the shear fabric and is related to upright folds that overprint the shear zones in the Mont Chétif massif, marking the end of ductile shearing (Figure 3d). DE05 has a matrix that consists mainly of fine-grained (10–20 μm on average) white mica, quartz, K-feldspar, and albite, with regularly

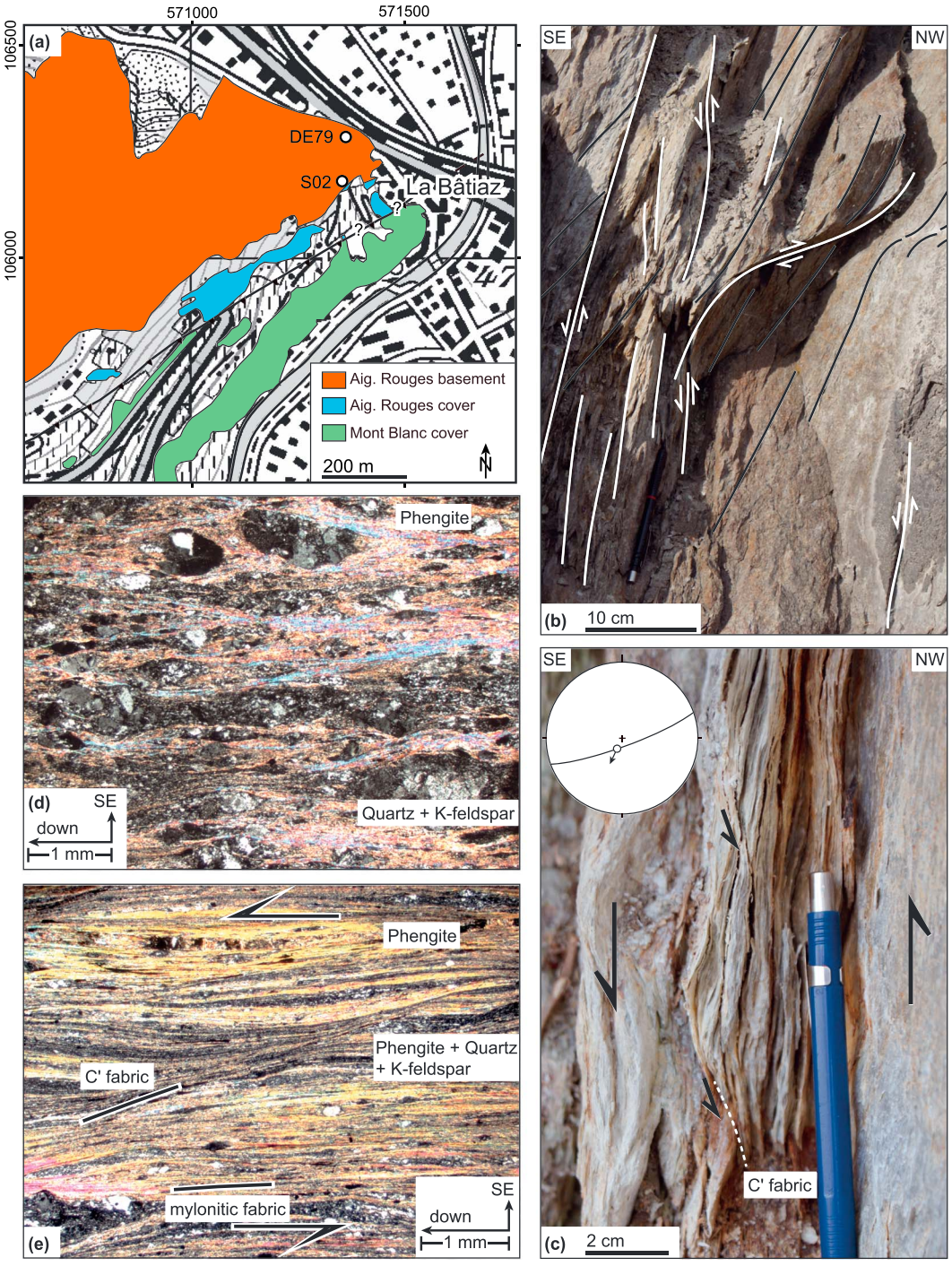

Figure 4. Field observations, sample locations, and microphotographs from La Bâtiaz: (a) Geological map redrawn after geological map of Switzerland (1:25000, sheet Sembrancher, Swiss coordinates). The exact location of the contact between the covers of Mont Blanc and Aiguilles Rouges is speculative. (b) Typical appearance of the conjugate shear zones overprinting the earlier Alpine fabric (46.10841, 7.06811). (c) Sample location of S02. The entire phyllonitic zone is ~1 m wide and shows a consistent SE down sense of shear (46.10666, 7.06827). (d) Microphotograph of sample DE79 indicating NW directed shear on mica-rich shear bands but only weak recrystallization. (e) Microphotograph of sample S02 showing large white mica domains and shear bands indicating SE down movements.

distributed large albite and K-feldspar clasts (0.5 to >1 mm) and foliation-parallel quartz domains (Figure 3c). The matrix often shows an intergrowth of white mica, feldspar, and quartz, but relatively pure domains of white mica can still be found. DE37 is comparable to DE05 but shows less intergrowth, and white micas are well recrystallized within the foliation, forming new grains of 10–50 μm thickness and several hundred micrometer in diameter (Figure 3d).

5.2. NE Aiguilles Rouges Massif (La Bâtiaz)

The eastern margin of the Aiguilles Rouges massif at La Bâtiaz (Martigny) in the Swiss Rhône Valley (Figure 4a) is characterized by an intense schistosity. Two types of ductile Alpine deformation can be distinguished. A pervasive mylonitic fabric is oriented ~120/70 (dip direction/dip) and shows consistent top-to-NW transport, presumably associated with movements along the basal thrust of the Morcles nappe. This deformation extends for ~100 m into the Aiguilles Rouges basement to the west and shows a strong gradient from (ultra) mylonites to largely unaffected Pre-Mesozoic gneiss [*Ayrton*, 1980]. This main fabric is overprinted by a series of steep, less than millimeter- to decimeter-wide, SW-NE striking mylonitic and phyllonitic shear zones, often forming conjugate sets with a large intersection angle containing the shortening direction (Figure 4b). The current orientation of these shear zones corresponds to normal fault kinematics, but orogen-perpendicular extension is unlikely considering the overall tectonic setting. They are thus interpreted as overturned steep conjugate reverse fault sets, reflecting an increased pure shear component to the deformation subsequent to NW directed shear [*Egli and Mancktelow*, 2013; *Egli et al.*, 2016]. Toward the basement-cover boundary to the east, the overprint of these shear zones is increasingly prevalent and largely dominated by the fault set showing SE down kinematics. The boundary between the Aiguilles Rouges basement and its sedimentary cover is marked by a meter-wide shear zone with an exclusively SE down sense of movement (Figure 4c), which locally implies a relative uplift of Aiguilles Rouges with respect to the Chamonix zone and Mont Blanc massif. Sample DE79 was collected from a zone showing top-NW shearing and is characterized by layers of cataclastic feldspars sandwiched between a fine-grained matrix of relatively pure white mica aggregates, with some intergrowth of quartz, K-feldspar, and plagioclase (Figure 4d). Sample S02 appears to be fully synkinematically recrystallized during the later SE down phyllonitization overprint, and no remnants of the earlier deformation can be observed (Figure 4e). It mainly consists of relatively large (0.5 to >1 mm) flakes of white mica with smaller fragments and layers of quartzo-feldspathic material. From sample S02, two grain-size fractions (160–250 μm and 250–500 μm) were separated and analyzed.

5.3. NE Belledonne Massif (Beaufort-Roselend Area)

The Belledonne massif is composed of an internal and an external zone, separated by a narrow strip of Mesozoic sediments, referred to as the median fault or accident médiane [*Antoine et al.*, 1992]. The median fault can be considered to be the southern continuation of the Chamonix zone, which splits into several splays south of the Chamonix valley and separates the internal and external parts of Belledonne. Two samples from the Beaufort-Roselend region were collected from the northern part of the internal Belledonne massif (Figure 5a). The northern end of the internal Belledonne massif is of heterogeneous composition, with a variety of orthogneiss and paragneiss slices separated by thrusts and, at times, also by narrow bands of Mesozoic cover. In the Beaufort area, two splays of the median fault can be observed and the tectonic position is comparable to the situation at La Bâtiaz. The structural appearance of the more recent tectonic overprint is also quite similar: many localized small-scale faults can be observed, predominantly showing oblique dextral SE down movements but often with conjugate counterparts. Larger phyllonitic zones are developed infrequently. Sample DE56 was collected from a ~1 m wide phyllonitic shear zone developed in a strongly sheared orthogneiss 3 km east of Beaufort village. The shear zone dips subvertically to the west (fault plane: 276/83, stretching lineation: 216/70, and shear sense east side down) (Figure 5b). The surrounding rocks have a pervasive low-grade Alpine foliation with dominantly SE down shear sense criteria. This sheared domain is separated from another basement unit to the east by a ~100 m wide zone of Triassic sediments. Sample DE68 was collected from a thin subvertical phyllonitic zone from this more internal exposure of basement rocks (fault plane: 136/88, stretching lineation: 228/70, and shear sense SE side down) 500 m NW of Lac de Roselend (Figure 5c). Although the surrounding rocks often show an Alpine overprint, it is less pervasive than at location DE56 and reflects top-to-NW shear. The two analyzed samples are rather dissimilar, which reflects the difference in Alpine deformation overprint. DE56, which has a phyllonitic appearance in hand specimen, shows a finely intergrown matrix of white mica, quartz, K-feldspar, and plagioclase and with roughly

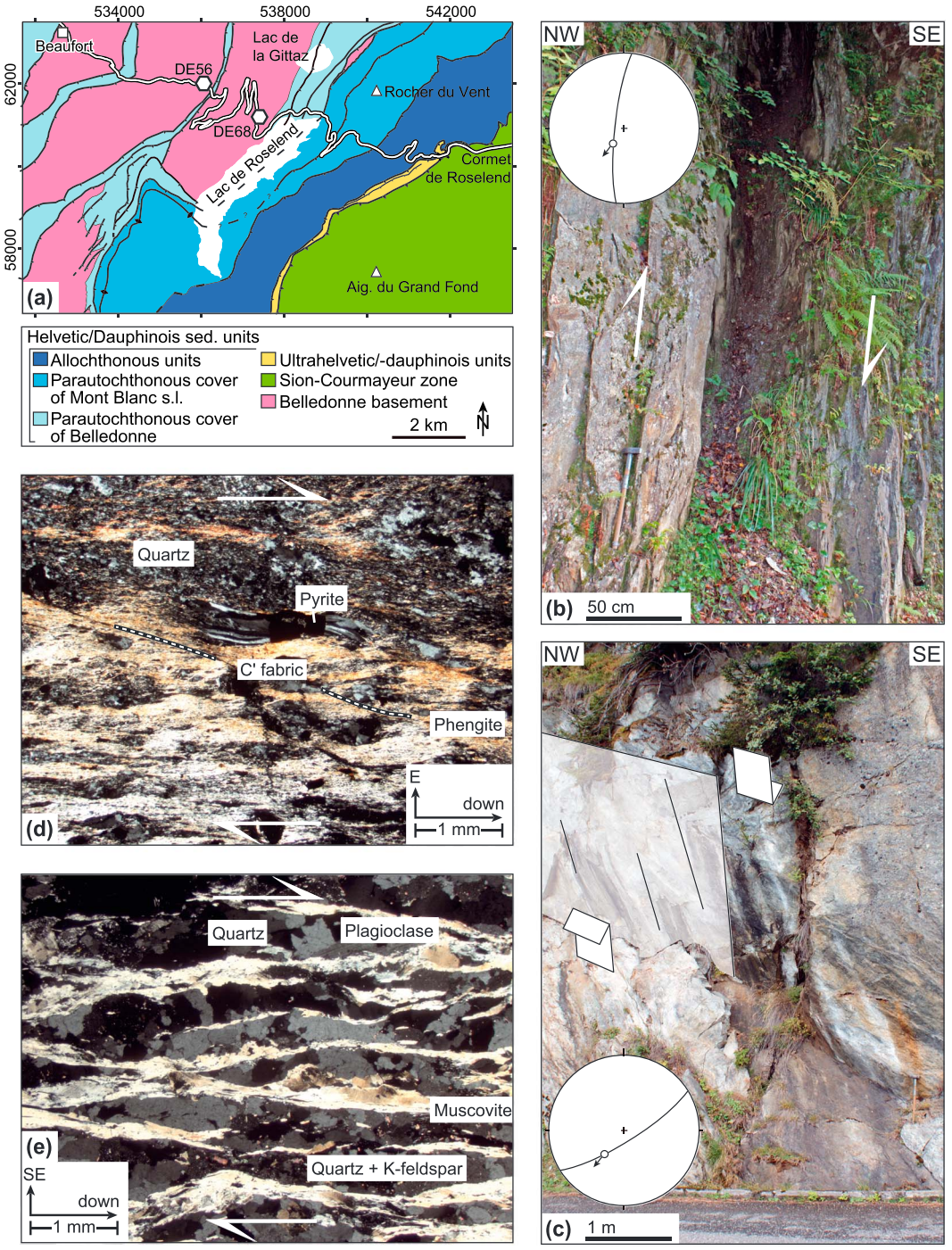

Figure 5. Field observations, sample locations, and microphotographs from the Beaufort-Roselend area: (a) Tectonic map redrawn after geological map of France (1:25000, sheet Bourg-St-Maurice, Swiss coordinates). (b) Sample location and fault orientation of DE56 (45.70566, 6.61956). The internal structure of the fault indicates SE down sense of shear. Image flipped horizontally. (c) Sample location and fault orientation of DE68. Brittle shear sense indicators show SE down movements (45.70040, 6.63386). (d) Microphotograph of sample DE56 showing strong recrystallization and a SE down shear sense. (e) Microphotograph of sample DE68 showing only minor recrystallization and large domains of old muscovite.

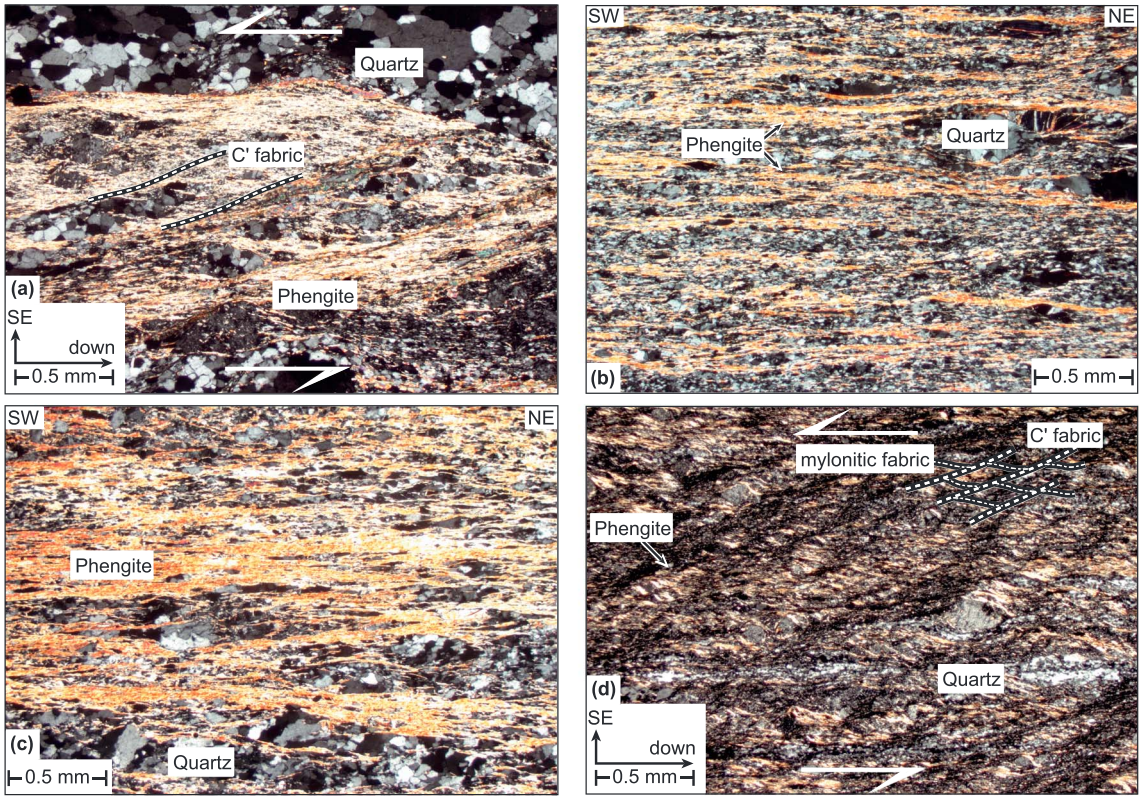

Figure 6. Microphotographs of the analyzed samples: (a) Sample DE65 showing broad domains of synkinematic phengite in shear bands indicating top-NW movement. (b) DE59 from the metasediments of the Sion-Courmayeur zone showing a pervasive shear fabric of quartz and phengite. (c) Sample DE64 is comparable to DE59 but with larger phengite aggregates. (d) DE73 shows an ultramylonitic fabric with oblique top-NW and dextral sense of shear with a well-developed shear band fabric.

10–50 μm sized grains. Layers of pure mica ~0.5 to 1 mm thick form in between quartz-rich layers (Figure 5d). DE68 has a more homogeneous grain-size distribution and is relatively coarse-grained, with >1 mm white mica, quartz, K-feldspar, and plagioclase (Figure 5e). Although a foliation plane is well defined by the mica and quartz-feldspar layers, no significant recrystallization or grain-size reduction appears to have taken place. For both samples DE56 and 68, two grain-size fractions (100–160 μm and 160–250 μm) have been analyzed.

5.4. N Mont Blanc Massif (Faille du Midi)

Sample DE65 was collected along the road from Champex-Lac toward Les Valettes, close to the contact between the Mont Blanc granite and the Variscan paragneiss (Faille du Midi or Faille d'Angle [*Bellière*, 1988]). It strikes NE-SW, parallel to the Chamonix valley, and runs along the entire length of the massif from Mont Chemin north of Sembrancher to the Roselend area in the south, bisecting the massif into an internal and an external zone [e.g., *Epard*, 1990]. In the northern parts of the Mont Blanc massif, it forms the boundary between the Mont Blanc granite and the amphibolite-facies Variscan paragneisses, whereas from roughly east of Chamonix (Plan de l'Aiguille) southward it crosscuts only the Variscan gneisses [*Corbin and Oulianoff*, 1926; *Steck et al.*, 2001]. It is supposed to be the major feature along which the Mont Blanc granite moved upward during emplacement [*Bellière*, 1988], followed by repeated mylonitization of at least parts of the contact, resulting in a few meters to up to ~100 m wide shear zone [*Corbin and Oulianoff*, 1926]. Alpine low-grade thrusting along localized shear zones, possibly also reactivating the Faille du Midi, is very common in the Mont Blanc basement [*Bellière*, 1988; *Rossi et al.*, 2005; *Rolland et al.*, 2008]. The sample was collected from a phyllonitic shear zone located in the Mont Blanc orthogneiss in close proximity to the protolith boundary to the paragneiss. The phyllonitic foliation is oriented 128/88, and the lineation plunges 037/49, showing an oblique dextral and top-to-NW sense of shear. The collected sample DE65 is mainly composed of quartz and white mica. Large amounts of white mica define the foliation plane, and pure mica aggregates of

100–500 μm thickness occur parallel to the foliation and in C′ shear bands (Figure 6a). Two grain-size fractions (100–160 μm and 160–250 μm) have been separated and analyzed for DE65.

5.5. Sion-Courmayeur Zone (Col de la Seigne)

Samples DE64 and DE59 were collected from strongly sheared metasediments of the Sion-Courmayeur zone in the hanging wall of the Penninic thrust on Col de la Seigne at the border between Italy and France, ~500 m from the protolith boundary between Helvetic units and the Sion-Courmayeur zone (Figure 1). The entire rock mass is affected by pervasive mylonitization, and no smaller-scale localized shear zones are observed. The mylonitic fabric dips to the SE (151/42) and shows a shallow SW dipping stretching lineation (213/14), with an oblique top-to-north movement. Both samples almost entirely consist of quartz and white mica, which define the foliation plane. DE59 shows mica domains of ~20–50 μm thickness, with single crystals of up to 200 μm diameter. The quartz domains and subgrains are flattened in the foliation plane, with grains of ~50 μm size (Figure 6b). DE64 is comparable to DE59, although grain sizes are less homogenous, with a tendency for coarser grains in quartz-rich domains and smaller grains where quartz and mica are intergrown. Pure white mica aggregates can have a thickness of 500 μm or more and form continuous layers (Figure 6c).

5.6. E Aiguilles Rouges Massif (Miéville Shear Zone, Vallorcine)

The Miéville shear zone marks the eastern border of the Vallorcine granite in the Aiguilles Rouges massif. It has been studied extensively in terms of microstructures, geochemistry, and geochronology [e.g., *Reinhard and Preiswerk*, 1927; *Steck and Vocat*, 1973; *Kerrich et al.*, 1980; *Fitz Gerald and Stunitz*, 1993]. Although its main activity is generally assumed to be pre-Alpine, its tectonic context and its significance for the Alpine evolution are a matter of debate. The sample site lies in the prolongation of the shear zone sampled by *Rolland et al.* [2008] at Châtelard, which they incorrectly correlated with the Mont Blanc shear zone and hence the Mont Blanc massif. Their data, as well as field observations, indicate Alpine reactivation along this part of the shear zone, although these observations cannot necessarily be extrapolated to the entire shear zone. Sample DE73 was collected in the southern prolongation of this structure, east of the village of Vallorcine, and shows an oblique top-to-NW sense of movement with a dextral component (mylonitic foliation: 124/67 and stretching lineation 053/39). The rock is an ultramylonite of granitic origin with feldspar porphyroclasts of ~200 μm size and a matrix that consists of ~10 μm quartz, plagioclase, and K-feldspar grains. About 50 vol % of the rock consists of white mica with a thickness of 10–50 μm and a diameter of 100–400 μm (Figure 6d).

6. Results

6.1. General Remarks

In general, two types of useful Ar-age spectra were obtained in this study. The ideal case is that with a single undisturbed plateau age, but unfortunately, this was found in only 5 of the total 14 analyses. The most common results (six analyses) were age spectra that show a general increase in age toward higher-temperature steps. High apparent Ar-ages in the first low-temperature steps are interpreted as release of excess ^{40}Ar and therefore had to be discarded. All samples showed very high amounts of radiogenic Ar, leading to insufficient spread on the inverse isochron plots and therefore meaningless results for the intercept. However, age calculations from the inverse isochrons generally correspond to the plateau ages within error. Only one sample (DE59) had to be completely discarded due to recoil, whereas two samples (DE68 and DE68b) yielded useful information despite disturbed apparent age spectra (see below).

Staircase spectra can be interpreted as mixing lines between two extreme values corresponding to different events, as the result of slow cooling through the closure window, as due to punctuated periods of shear or reheating of already closed systems, or as a combination of any of these mechanisms [e.g., *Villa*, 1998]. Single events could be (i) cooling below the closure temperature, (ii) shear and/or increased fluid flow leading to recrystallization or neocrystallization, and (iii) resetting due to reheating, fluid flow, or alteration (mechanical or chemical) of the grains. If two or more of these events occur but do not individually completely reset the previous isotope composition, staircase spectra are to be expected. Every age step represents a minimum age (except in the case of excess Ar), and the possibility of age reduction by one of the above mentioned processes has to be considered. The complete data table can be found in Table S1 in the supporting information.

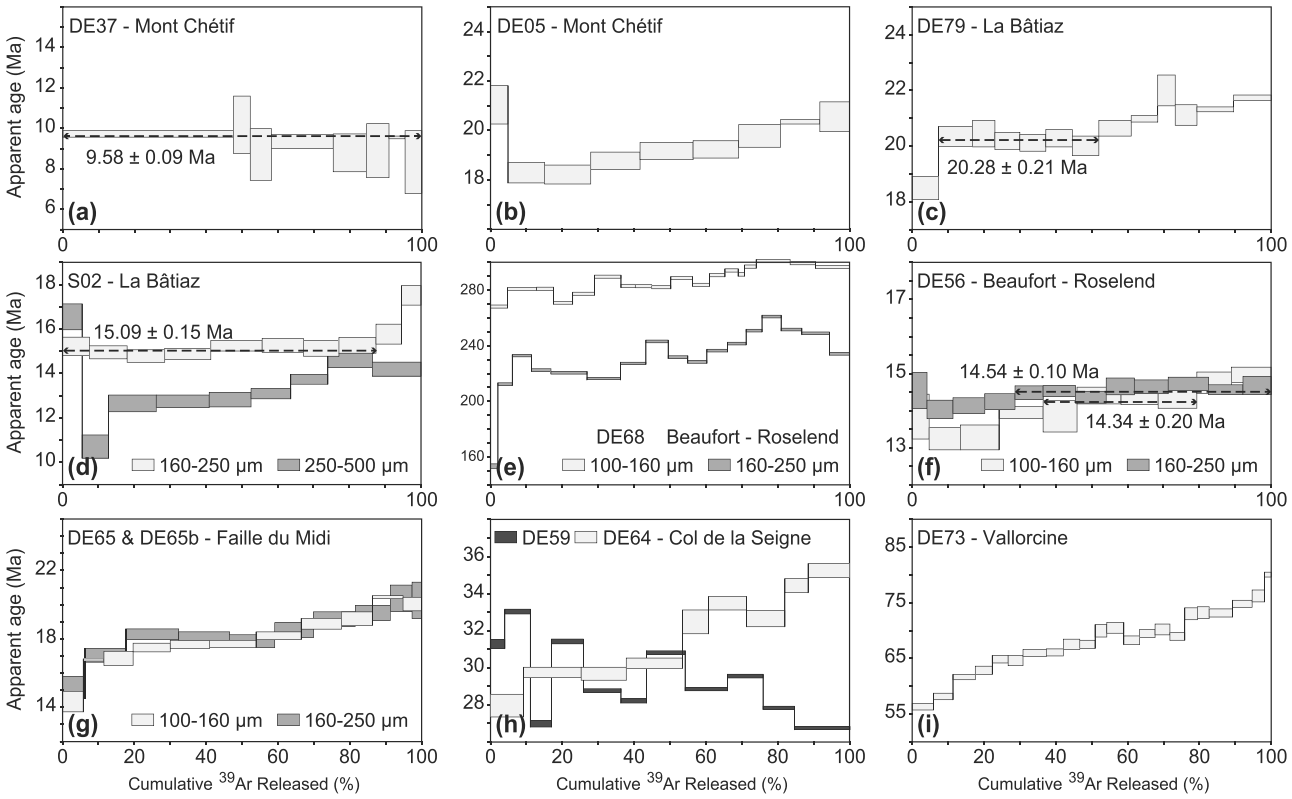

Figure 7. $^{40}Ar/^{39}Ar$ apparent age spectra of the analyzed samples.

6.2. Analyses

The results of the $^{40}Ar/^{39}Ar$ analyses are summarized in Table 1. Samples DE05 and DE37 from the Mont Chétif basement both yield good results with small errors as well as identical normal and inverse isochron ages within error. Sample DE37 shows one single plateau age of 9.58 ± 0.09 Ma, indicating a discrete rejuvenation event (Figure 7a). Sample DE05 yielded an age spectrum between 18 and 21 Ma, with the first heating step releasing excess Ar (Figure 7b). Despite their close proximity (200 m) at the same elevation, these samples show distinctively different ages, indicating that their isotopic systems did not close simultaneously and that DE37 was rejuvenated, whereas DE05 was unaffected by the more recent event. The younger age of DE37 is therefore most likely due to synkinematic recrystallization of the micas below their closure temperature, completely resetting the older isotopic system. For sample DE05, the apparent age spectrum is more disturbed and the interpretation thus more complicated. However, the spread of ages is rather small and is interpreted to reflect relatively slow cooling through the closure window between 20 and 18 Ma. The apparent K/Ca ratio shows slightly different values for two high-*T* steps, as well as for the first low-*T* step (excluding the first step that shows excess Ar). This might be an effect of contamination of the aggregates by fragments of other minerals (e.g., K-feldspar), which would degas at higher temperatures. Alternatively, remnants of an older isotopic system in the core of the grains with a slightly different chemistry could lead to the slightly higher ages in the two high-*T* steps.

The two samples from La Bâtiaz S02 and DE79 both yielded results with plateaus in the apparent age spectra. Sample DE79, which consists of white mica from the main Alpine low-grade fabric, yielded a plateau with 60% of gas released at 20.28 ± 0.21 Ma and shows a minor increase in age toward the high-*T* steps (Figure 7c). The significantly younger first heating step indicates minor chemical or mechanical alteration. For sample S02, two grain-size fractions were analyzed and the 160–250 µm fraction gave an undisturbed plateau at 15.09 ± 0.15 Ma with ~90% of gas released (Figure 7d). The 250–500 µm fraction showed a more disturbed spectrum with a younger apparent total fusion age, possibly related to chemical alteration, and was therefore discarded. This could be because the larger fraction formed aggregates of several smaller grains rather than single large grains, and these aggregates of finer grains would be more prone to chemical alteration.

Of the two samples from the Beaufort-Roselend area, two grain-size fractions were analyzed. The two analyses of sample DE68 gave total fusion ages of 287 Ma and 235 Ma, respectively (Figure 7e). The erratic spectra indicate thermal, mechanical, and/or chemical alteration. However, significant Alpine thermal or synkinematic resetting of the grains can be excluded due to their Permian apparent age. The horizontal distance to sample DE56 is only 1200 m, but the ages are completely different, indicating that regional Alpine metamorphism did not reach temperatures high enough to thermally reset the isotopic system. For sample DE56, the 160–250 μm fraction yielded a significant plateau for the higher-*T* steps with more than 70% of Ar released at 14.54 ± 0.1 Ma and a slight decrease in age for the low-*T* steps down to ~14 Ma (Figure 7f). Isochron ages are identical within error. The first step is disturbed by excess Ar. The 100–160 μm fraction shows a similar spectrum from 15 to 13 Ma but only forms a miniplateau at 15.34 ± 0.2 Ma. The distinctive staircase-plateau combination of the DE56b is interpreted as due to mechanical grain-size reduction subsequent to homogeneous rejuvenation.

The two grain-size fractions from sample DE65 from the northern Mont Blanc massif gave identical staircase spectra between ~17 and 20.5 Ma with a significantly younger first step (14 Ma and 15 Ma, respectively), which does not lie on the trend of the staircase spectrum. In both fractions, a miniplateau at ~18 Ma is seen (Figure 7g). The youngest steps off the mixing line could represent alteration or new growth of micas, but we favor the scenario of Ar loss due to alteration (mechanical or chemical) in the rims of the grains, thereby resulting in apparent ages that are too young in the low-temperature steps. Slight variations in the K/Ca ratios toward the high-*T* steps indicate varying compositions and possibly reflect preserved older ages in the cores of the grains.

The two samples from Col de la Seigne are located within the deformation zone of the Penninic thrust, 500 m from the lithological boundary between the Sion-Courmayeur zone and the Helvetic metasediments. Sample DE59 yielded a completely meaningless spectrum, which can be an effect of either recoil or alteration; the analysis had to be discarded (Figure 7h). Sample DE64, collected at the same locality showed an age spectrum between 28 and 35 Ma with a miniplateau at 30 Ma (Figure 7h).

For sample DE73, the amount of gas released was remarkably high and the spectrum is therefore composed of 22 steps (Figure 7i). The almost linear spread of apparent ages ranges from 56 to 80 Ma, and a similarly linear minor decrease of the apparent K/Ca ratio can be observed. The spectrum most probably represents a mixing between older ages and final closure at around 56 Ma.

7. Discussion

The controlling factors for isotopic closure need to be considered in order to understand the relevance of the ages obtained in this study. Although most of the sampled shear zones appear to have been active under low-grade (epizonal to lower greenschist facies) conditions, temperatures after the activity of the shear zones might have been high enough to allow for thermally induced isotopic diffusion. In this case the ages obtained would reflect the time of cooling below the closure window rather than neocrystallization or recrystallization. Younger ages from samples located in close proximity to samples showing older ages, as is the case for samples DE37, S02, DE56, and DE56b, are interpreted to represent the time of recrystallization or neocrystallization during shear zone activity. Even though in the case of DE37 the degassing steps are somewhat irregular, a rejuvenation of the isotopic system around the time given by the apparent plateau age (9.58 ± 0.09 Ma) seems a justifiable interpretation. The fact that sample DE05, which was collected only 200 m away from DE37, shows a significantly higher $^{40}Ar/^{39}Ar$ age (18–20 Ma), indicates that temperatures in the Mont Chétif were below the closure window for white mica after that time. The resetting of the grains of DE37 is therefore interpreted to reflect the activity of the phyllonitic shear zone and associated white mica neocrystallization or recrystallization.

Rb-Sr ages obtained from sample DE05 range from 26 to 33 Ma [*Egli et al.*, 2016] and therefore show ages roughly 10 Ma older than the $^{40}Ar/^{39}Ar$ age from the same sample. If both systems were reset synkinematically below the closure temperature for the $^{40}Ar/^{39}Ar$ system, identical ages would be expected, which is not the case. However, because laser-cut Rb-Sr microsampling allowed dating of dynamically newly crystallized phases, these ages are interpreted as formation ages during an early period of deformation [*Egli et al.*, 2016], whereas the 18–20 Ma $^{40}Ar/^{39}Ar$ ages are interpreted as cooling of the Mont Chétif below the generally

proposed closure temperature of ~350 ± 50°C [e.g., *Dodson*, 1973]. It is notable that the apparent $^{40}Ar/^{39}Ar$ age range of sample DE64 is also similar to the Rb-Sr ages of DE05 [*Egli et al.*, 2016] and corresponds to allanite ages from the central Mont Blanc massif [*Cenki-Tok et al.*, 2014]. The relatively wide spread in this spectrum (28–35 Ma) does not allow an obvious interpretation. However, the staircase spectrum could represent a mixing line between an unknown inherited age before 35 Ma and partial resetting, possibly related to recrystallization due to deformation along the Penninic thrust in Oligocene times. If the apparent ages are considered as minimum ages, then it follows that there was no regional thermal overprint at this location after ~28 Ma.

The apparent ages obtained from La Bâtiaz (DE79 and S02) show a wide spread, and their interpretation is not straightforward. Temperatures in the northern Aiguilles Rouges massif have reached temperatures high enough to cause partial resetting of the zircon fission track system [*Soom*, 1990]. However, although partial opening of the biotite K/Ar isotopic system might have occurred, temperatures significantly above 300°C are unlikely during Alpine metamorphism. Maximum temperature estimates by *Kirschner et al.* [1995, 1996] are around 320–330°C and estimates by *Boutoux et al.* [2016] using RSCM thermometry are also around 300°C. It is therefore proposed that both $^{40}Ar/^{39}Ar$ ages from La Bâtiaz represent formation ages rather than cooling ages. The miniplateau at 20.28 ± 0.21 Ma in sample DE79 and the slightly increasing ages toward the higher temperature steps are interpreted as dynamic resetting of pre-Triassic ages at ~20 Ma. Partially preserved older isotopic ratios in the cores of the grains would explain the observed staircase spectrum toward the high-*T* steps due to mixing of the two isotope ratios. The significantly younger first low-temperature step is interpreted as minor chemical or mechanical alteration of the rims of the grains. The structural context obtained from field and microstructural observations allows two schistosities related to different kinematics to be clearly distinguished, which can explain the difference in the $^{40}Ar/^{39}Ar$ apparent ages between DE79 and S02. The undisturbed plateau age of S02 at 15.09 ± 0.15 Ma is interpreted to relate to complete dynamic resetting of the older isotopic system during formation of the conjugate shear zones that overprint the earlier Alpine fabric at La Bâtiaz and other localities throughout the Chamonix zone.

The two grain size fractions from DE56 from the area south of the Chamonix valley yielded very similar ages to the one from S02, and considering the comparable tectonic position and kinematics, it is likely that they correspond to the same geodynamic setting. For the ages of DE56, an initial resetting of the grains during phyllonitization at ~14.5 Ma and subsequent Ar release due to mechanical grain-size reduction (or chemical alteration) down to ~13 Ma is proposed to explain the slight drop in ages in the low-temperature steps. The two age gradients obtained from the two grain-size fractions of sample DE65 from the Faille du Midi show slightly younger ages than published K/Ar biotite ages from the central Mont Blanc massif [*Leloup et al.*, 2005], implying that the isotopic system was reset below its "closure window." The miniplateau, which in both fractions lies between 17 and 18 Ma, could therefore represent a period of recrystallization of older micas from the granite, which had an older cooling age that is partly preserved in the core of the grains, thereby producing the staircase-type increase of age toward the high-temperature steps. The significantly younger first low-temperature step is interpreted as mechanical or chemical alteration. However, although the sample location lies on the Faille du Midi, it is not obvious whether this is only a local phenomenon or whether this Miocene reactivation can be extrapolated to the entire length of the Faille du Midi.

For sample DE73, no unequivocal interpretation can be proposed. The large gradient in ages indicates either a mixing of two discrete events or slow cooling of the micas between 56 and 80 Ma. The interpretation is therefore limited to the observation that the isotopic system closed at a minimum time of 56 Ma and that no further significant alteration of the grains took place after that time.

Structures indicating uplift of the Aiguilles Rouges massif relative to the Mont Blanc massif can be observed in several localities along the eastern margin of the Aiguilles Rouges and internal Belledonne massifs, often expressed as conjugate shear zones with dominant SE down kinematics. The ages from La Bâtiaz and Beaufort suggest that this localized relative motion between Aiguilles Rouges and Mont Blanc occurred at around 14.5–15 Ma. These shear zones may have developed due to internal deformation related to extrusion and updoming of the Aiguilles Rouges massif above a basal thrust below its north-western flank [*Lacassin*, 1989; *Burkhard and Sommaruga*, 1998; *Leloup et al.*, 2005]. Two ages from the Chamonix zone from other studies lie also in this time window, and an alternative interpretation for sample 92-29J of *Kirschner et al.* [1996] and sample S68 of *Rolland et al.* [2008] is proposed here. Sample 92-29J from the mylonitic limestones at

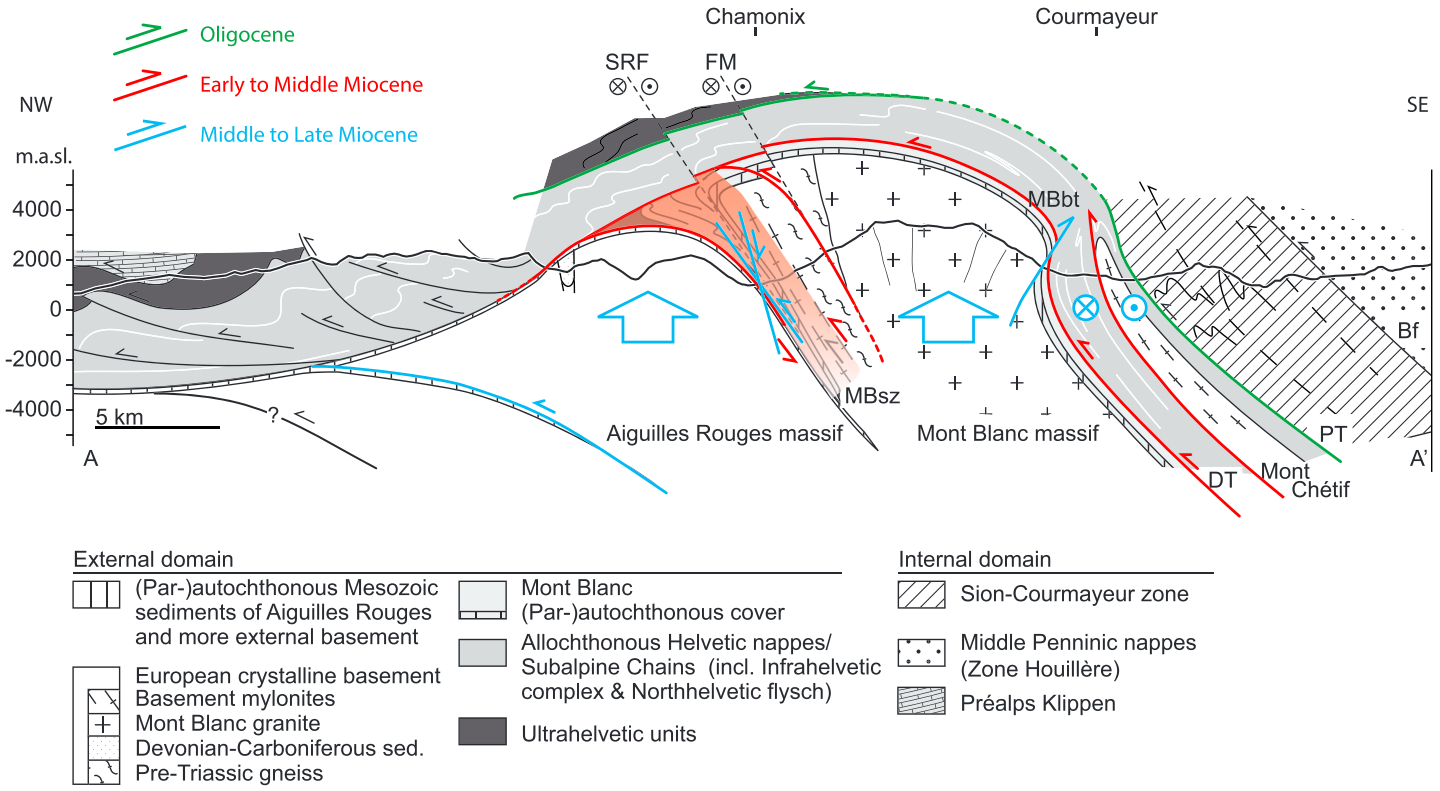

Figure 8. The major faults discussed in this study in their present-day position, color-coded according to their main phase of activity. The most important kinematic reconfiguration is interpreted to take place during the Middle Miocene when major NW directed movements were replaced by more coaxial shortening and the main thrust front shifted further to the NW below the Aiguilles Rouges massif.

La Bâtiaz (Masson, personal communication) shows youngest apparent age steps around 15–16 Ma, and sample S68 has a miniplateau at 14.3 ± 0.2 Ma. The latter sample is located at Châtelard at the border between France and Switzerland and corresponds to the still enigmatic Miéville shear zone. The Miéville shear zone has a complex history and supposedly has been active in both pre-Alpine and Alpine times [e.g., *Chessex et al.*, 1962; *Steck and Vocat*, 1973]. The field and microstructural observations demonstrate that the shear zone at Châtelard shows SE down movements comparable to what is observed at Bâtiaz, the Aiguillette des Posettes, Beaufort, and other localities along the Chamonix zone [*Egli and Mancktelow*, 2013]. The age of 14.3 ± 0.2 Ma from sample S68 [*Rolland et al.*, 2008] corresponds to the newly obtained ages from Beaufort within error and is only slightly younger than the results from La Bâtiaz. However, only 1200 m south along the strike of the same structure, DE73 does not appear to have been reset during Miocene times, and therefore, reactivation is rather localized and does not affect the entire shear zone.

8. Regional Geologic Implications and Conclusions

The tectonic evolution of the study area can be considered in terms of an overall in-sequence history of thrusting on (1) the Penninic thrust in Oligocene times, (2) the Diablerets thrust, (3) the Mont Blanc shear zone (or Morcles thrust north of the Rhône valley), and (4) a proposed basal blind thrust below the Aiguilles Rouges/Infra Rouges massifs, with further translation of the deformation into the Jura mountains (Figure 8) [e.g., *Ramsay et al.*, 1983; *Crespo-Blanc et al.*, 1995; *Kirschner et al.*, 1995, 1996; *Burkhard and Sommaruga*, 1998; *Ceriani et al.*, 2001; *Simon-Labric et al.*, 2009]. The early stage of deformation in Oligocene times is followed by outward propagation of the deformation front leading to uplift in the hanging wall of these thrusts, which is accompanied by out-of-sequence activity along several localized shear zones between the Penninic thrust and the Alpine orogenic deformation front, as well as by the formation of a regionally pervasive S2 schistosity [*Egli and Mancktelow*, 2013]. Initiation of burial of the Helvetic domain is recorded by the Oligocene deformation ages on the Penninic thrust and in its footwall. Onset of cooling and uplift of the

Mont Blanc massif is related to NW directed thrusting along the major tectonic contacts interpreted to have been active in Early Miocene times [*Kirschner et al.*, 1995; *Glotzbach et al.*, 2011; *Boutoux et al.*, 2016]. Cooling of the Mont Chétif massif below ~350°C at around 18–20 Ma may therefore be related to NW directed thrusting along shear zones such as the Diablerets thrust, the Faille du Midi (DE65), and the Mont Blanc shear zone/Morcles thrust (DE79). The end of significant NW directed thrusting is considered to be between 17–19 Ma for the Morcles thrust [*Kirschner et al.*, 1995] and ~15 Ma for the Diablerets thrust [*Crespo-Blanc et al.*, 1995]. This may be due to transfer of the main thrusting of the external zone onto a basal thrust below the Aiguilles Rouges massif [e.g., *Lacassin*, 1989; *Burkhard and Sommaruga*, 1998; *Leloup et al.*, 2005; *Bellahsen et al.*, 2014] causing updoming of the Aiguilles Rouges and Mont Blanc basement stack and largely deactivating the uplifted and bent earlier thrusts. The Aiguilles Rouges basement would thereby be extruded between this basal thrust and the overlying Mont Blanc basement, possibly associated with an overall updoming and hinterland-directed tilting of the entire system. Related internal deformation was probably accommodated along shear zones in the Chamonix zone and reactivation of preexisting structures such as the Miéville shear zone and the basement-cover interface at 14.5–15 Ma (DE56 and S02). Top-to-SE shear zones related to the Mont Blanc back thrust, which are described to be active at ~16 Ma [*Rolland et al.*, 2007], might represent a slightly earlier equivalent scenario for the Mont Blanc massif. An interaction as large-scale conjugate shear systems during the early stages of updoming of the basement massifs is therefore proposed.

This proposed structural relationship is not in immediate accord with low-temperature thermochronology data published for the mid-Miocene. During the period of 15–12 Ma, the Mont Blanc massif records rapid uplift and cooling [e.g., *Glotzbach et al.*, 2008, 2011] whereas the single published ZFT age for the Aiguilles Rouges massif might indicate earlier (~17 Ma) cooling [*Soom*, 1990]. This could be explained by one or a combination of the following: (i) a rather short-lived activity of SE down movements between Mont Blanc and Aiguilles Rouges followed by rapid uplift of Mont Blanc, (ii) SE down movements being of only minor importance for the overall uplift of the two massifs and/or compensated by conjugate SE-up movements in the Chamonix zone or the Mont Blanc shear zone, (iii) the observed structures being mainly a result of tilting of the system and reconfiguration of the kinematic scenario from NW directed thrusting to more coaxial shortening, and (iv) the very limited ZFT data from the Aiguilles Rouges massif, with all other ZFT being nonreset [*Vernon et al.*, 2008] compared to the high data density in the Mont Blanc massif could result in a misinterpretation of the respective cooling histories of the two massifs.

Transverse upright folds with N-S striking steep axial planes overprint earlier structures such as the Mont Blanc back thrust and the Mont Chétif shear zones [*Egli and Mancktelow*, 2013]. They most probably correspond to the formation of a N-S trending culmination that affected all structural units and was related to E-W compression, as described by *Ramsay* [1989]. From the current results for sample DE37 from the Mont Chétif massif, transcurrent ductile shearing has occurred until at least 9.5 Ma before being affected by these folds, so that this age gives a maximum time limit for initiation of this transverse folding. Considering back-folding and back thrusting to have initiated after ~15–16 Ma and the 9.5 Ma age for the shear zone overprinted by this steep fabric, the period of important back-folding/ backthrusting had to occur somewhere in this range of approximately 15–9.5 Ma. The young shear zones in the Mont Chétif massif are interpreted to reflect accommodation of NW directed shortening by strain partitioning along E-W oriented strike-slip zones during back-folding/ back thrusting and related updoming of the external crystalline massifs.

The new data obtained from $^{40}Ar/^{39}Ar$ geochronology applied to shear zones in the Mont Blanc-Aiguilles Rouges area provide important additional constraints on the cooling and deformation history of the region. The samples from Mont Chétif indicate that initial ductile shearing occurred in Early to mid-Oligocene times, corresponding to the onset of deformation in the upper Helvetic units and on the Penninic thrust, with subsequent cooling starting in Early Miocene. However, ductile movements along localized shear zones continued until at least Middle to Late Miocene times. From ~15 Ma, deformation on steep conjugate reverse faults is interpreted to accommodate internal deformation related to thrusting below the Aiguilles Rouges massif and related hinterland tilting and updoming of the entire Aiguilles Rouges and Mont Blanc region. Dextral transcurrent motion east of the Mont Blanc massif is an effect of strain partitioning of the overall WNW-ESE shortening on this more WSW-ENE trending segment, with this trend predefined by the already existing shape of the massif. Transcurrent shearing, possibly related to the Rhône-Simplon fault system lasted until at least ~9.5 Ma, followed by open transverse folding that was superposed across the entire region.

Acknowledgments
The data used are listed in the references, tables, and supporting information. This study was part of the collaborative Topo-Alps project under the auspices of the European Science Foundation (ESF) Eurocores Programme TOPO-EUROPE and was funded by the Swiss National Science Foundation (SNF projects 200021-134469 and 20TO21-120502). We thank C. Glotzbach and one anonymous reviewer for positive and constructive comments as well as Associate Editor E. Willingshofer and Editor C. Faccenna for additional input and manuscript handling.

References

Antoine, P., J. C. Barfety, J. Vivier, J. Debelmas, J. Desmons, H. Fabre, H. Loubat, and C. Vauterelle (1992), *Notice Explicative de la Feuille Bourg-Saint-Maurice à 1/50000*, 110 pp., BRGM, Orléans.

Aprahamian, J. (1988), Cartographie du métamorphisme faible à très faible dans les Alpes françaises externes par l'utilisation de la cristallinité de l'illite, *Geodin. Acta*, *2*(1), 25–32.

Ayrton, S. (1980), La geologie de la zone Martigny-Chamonix (versant suisse) et l'origine de la nappe de Morcles (un exemple de subduction continentale), *Eclogae Geol. Helv.*, *73*(1), 137–172.

Bellahsen, N., F. Mouthereau, A. Boutoux, M. Bellanger, O. Lacombe, L. Jolivet, and Y. Rolland (2014), Collision kinematics in the western external Alps, *Tectonics*, *33*, 1055–1088, doi:10.1002/2013TC003453.

Bellière, J. (1988), On the age of mylonites within the Mont Blanc massif, *Geodin. Acta*, *2*(1), 13–16.

Bogdanoff, S., A. Michard, M. Mansour, and G. Poupeau (2000), Apatite fission track analysis in the Argentera massif: Evidence of contrasting denudation rates in the external crystalline massifs of the Western Alps, *Terra Nova*, *12*(3), 117–125.

Boutoux, A., N. Bellahsen, U. Nanni, R. Pik, A. Verlaguet, Y. Rolland, and O. Lacombe (2016), Thermal and structural evolution of the external Western Alps: Insights from (U–Th–Sm)/He thermochronology and RSCM thermometry in the Aiguilles Rouges/Mont Blanc massifs, *Tectonophysics*, *683*, 109–123.

Burkhard, M. (1988), L'Helvétique de la bordure occidenale du massif de l'Aar (Évolution tectonique et métamorphique), *Eclogae Geol. Helv.*, *81*(1), 63–114.

Burkhard, M., and D. Goy-Eggenberger (2001), Near vertical iso-illite-crystallinity surfaces cross-cut the recumbent fold structure of the Morcles nappe, Swiss Alps, *Clay Miner.*, *36*(2), 159–170.

Burkhard, M., and A. Sommaruga (1998), Evolution of the western Swiss Molasse basin: Structural relations with the Alps and the Jura belt, *Geol. Soc. London, Spec. Publ.*, *134*(1), 279–298.

Cenki-Tok, B., J. R. Darling, Y. Rolland, B. Dhuime, and C. D. Storey (2014), Direct dating of mid-crustal shear zones with synkinematic allanite: New in situ U-Th-Pb geochronological approaches applied to the Mont Blanc massif, *Terra Nova*, *26*(1), 29–37.

Ceriani, S., B. Fugenschuh, and S. M. Schmid (2001), Multi-stage thrusting at the "Penninic front" in the Western Alps between Mont Blanc and Pelvoux massifs, *Int. J. Earth Sci.*, *90*(3), 685–702.

Chessex, R., F. De Montmollin, G. Ferrara, and A. Longinelli (1962), Measurements of the age of the Vallorcine granite (Switzerland), *Nature*, *193*(4822), 1279–1279.

Cliff, R. A., and S. Meffan-Main (2003), Evidence from Rb-Sr microsampling geochronology for the timing of Alpine deformation in the Sonnblick Dome, south-east Tauern window, Austria, in *Geochronology: Linking the Isotopic Record with Textures and Petrology*, edited by D. Vance, W. Müller, and I. Villa, *Geol. Soc. Spec. Publ.*, 159–172.

Corbin, P., and N. Oulianoff (1926), Les contacts, éruptif et mécanique, de la protogine et leur signification pour la tectonique du massif du Mont-Blanc, *Bull. Soc. Géol. Fr.*, *26*, 153–153.

Costa, S., and H. Maluski (1988), Use of the Ar-40-Ar-39 stepwise heating method for dating mylonite zones—An example from the St Barthelemy massif (northern Pyrenees, France), *Chem. Geol.*, *72*(2), 127–144.

Crespo-Blanc, A., H. Masson, Z. Sharp, M. Cosca, and J. Hunziker (1995), A stable and $^{40}Ar/^{39}Ar$ isotope study of a major thrust in the Helvetic nappes (Swiss Alps): Evidence for fluid flow and constraints on nappe kinematics, *Geol. Soc. Am. Bull.*, *107*(10), 1129–1144.

Dalrymple, B. G., and M. A. Lanphere (1974), $^{40}Ar/^{39}Ar$ age spectra of some undisturbed terrestrial samples, *Geochim. Cosmochim. Acta*, *38*(5), 715–738.

Dodson, M. H. (1973), Closure temperature in cooling geochronological and petrological systems, *Contrib. Mineral. Petrol.*, *40*(3), 259–274.

Dunlap, W. J. (1997), Neocrystallization or cooling? $^{40}Ar/^{39}Ar$ ages of white micas from low-grade mylonites, *Chem. Geol.*, *143*(3–4), 181–203.

Dunlap, W. J., C. Teyssier, I. McDougall, and S. Baldwin (1991), Ages of deformation from K/Ar and Ar-40/Ar-39 dating of white micas, *Geology*, *19*(12), 1213–1216.

Egli, D. (2013), Kinematics and timing of Alpine deformation in the Mont Blanc region (Western Alps), doctoral dissertation, 202 pp., ETH Zürich, Zürich, Switzerland.

Egli, D., and N. Mancktelow (2013), The structural history of the Mont Blanc massif with regard to models for its recent exhumation, *Swiss J. Geosci.*, *106*(3), 469–489.

Egli, D., W. Müller, and N. Mancktelow (2016), Laser-cut Rb–Sr microsampling dating of deformational events in the Mont Blanc-Aiguilles Rouges region (European Alps), *Terra Nova*, *28*(1), 35–42.

Eltchaninoff-Lancelot, C., S. Triboulet, B. Doudoux, S. Fudral, J.-P. Rampnoux, and M. Tardy (1982), Stratigraphie et tectonique des unités delphino-helvétiques comprises entre Mont-Blanc et Belledone (Savoie-Alpes occidentales): Implications régionales, *Bull. Soc. Géol. Fr.*, *24*, 817–830.

Epard, J.-L. (1990), La nappe de Morcles au sud-ouest du Mont-Blanc, *Mém. Géol. (Lausanne)*, *8*, 165.

Escher, A., H. Masson, and A. Steck (1993), Nappe geometry in the Western Swiss Alps, *J. Struct. Geol.*, *15*(3–5), 501–509.

Fitz Gerald, J. D., and H. Stunitz (1993), Deformation of Granitoids at low metamorphic grade 1. Reactions and grain-size reduction, *Tectonophysics*, *221*(3–4), 269–297.

Froitzheim, N., S. M. Schmid, and M. Frey (1996), Mesozoic paleogeography and the timing of eclogite-facies metamorphism in the Alps: A working hypothesis, *Eclogae Geol. Helv.*, *89*, 81–110.

Fügenschuh, B., and S. M. Schmid (2003), Late stages of deformation and exhumation of an orogen constrained by fission-track data: A case study in the Western Alps, *Geol. Soc. Am. Bull.*, *115*(11), 1425–1440.

Glotzbach, C., J. Reinecker, M. Danišík, M. Rahn, W. Frisch, and C. Spiegel (2008), Neogene exhumation history of the Mont Blanc massif, Western Alps, *Tectonics*, *27*, TC4011, doi:10.1029/2008TC002257.

Glotzbach, C., P. A. van der Beek, and C. Spiegel (2011), Episodic exhumation and relief growth in the Mont Blanc massif, Western Alps from numerical modelling of thermochronology data, *Earth Planet. Sci. Lett.*, *304*(3–4), 417–430.

Goy-Eggenberger, D. (1998), Faible métamorphisms de la nappe de Morcles: Minéralogie et géochimie, PhD thesis, Univ. de Neuchatel, Neuchatel, Switzerland.

Guermani, A., and G. Pennacchioni (1998), Brittle precursors of plastic deformation in a granite: An example from the Mont Blanc massif (Helvetic, Western Alps), *J. Struct. Geol.*, *20*(2–3), 135–148.

Hunziker, J. C., J. Desmons, and A. J. Hurford (1992), Thirty-two years of geochronological work in the central and Western Alps: A review on seven maps, *Mém. Géol. (Lausanne)*, *13*, 59.

Kempf, O., and O. A. Pfiffner (2004), Early Tertiary evolution of the north Alpine Foreland Basin of the Swiss Alps and adjoining areas, *Basin Res.*, *16*(4), 549–567.

Kerrich, R., I. Allison, R. L. Barnett, S. Moss, and J. Starkey (1980), Microstructural and chemical-transformations accompanying deformation of granite in a shear zone at Mieville, Switzerland—With implications for stress-corrosion cracking and superplastic flow, *Contrib. Mineral. Petrol.*, *73*(3), 221–242.

Kirschner, D. L., Z. D. Sharp, and H. Masson (1995), Oxygen isotope thermometry of quartz-calcite veins: Unraveling the thermal-tectonic history of the subgreenschist facies Morcles nappe (Swiss Alps), *Geol. Soc. Am. Bull.*, *107*(10), 1145–1156.

Kirschner, D. L., M. A. Cosca, H. Masson, and J. C. Hunziker (1996), Staircase $^{40}Ar/^{39}Ar$ spectra of fine-grained white mica: Timing and duration of deformation and empirical constraints on argon diffusion, *Geology*, *24*(8), 747–750.

Kirschner, D. L., H. Masson, and M. A. Cosca (2003), An $^{40}Ar/^{39}Ar$, Rb/Sr, and stable isotope study of micas in low-grade fold-and-thrust belt: An example from the Swiss Helvetic Alps, *Contrib. Mineral. Petrol.*, *145*(4), 460–480.

Koppers, A. A. P. (2002), ArArCALC—Software for $^{40}Ar/^{39}Ar$ age calculations, *Comput. Geosci.*, *28*(5), 605–619.

Lacassin, R. (1989), Plate-scale kinematics and compatibility of crustal shear zones in the Alps, *Geol. Soc. London, Spec. Publ.*, *45*(1), 339–352.

Leloup, P. H., N. Arnaud, E. R. Sobel, and R. Lacassin (2005), Alpine thermal and structural evolution of the highest external crystalline massif: The Mont Blanc, *Tectonics*, *24*, TC4002, doi:10.1029/2004TC001676.

Leloup, P. H., N. Arnaud, R. Lacassin, and E. R. Sobel (2007), Reply to comment by Y. Rolland et al. on "Alpine thermal and structural evolution of the highest external crystalline massif: The Mont Blanc", *Tectonics*, *26*, TC2015, doi:10.1029/2006TC001956.

Leutwein, F., B. Poty, J. Sonet, and J.-L. Zimmermann (1970), Age des cavités à cristeaux du granite du Mont Blanc, *C. R. Hebd. Seances Acad. Sci., Ser. D*, *271*(2), 156–158.

Mancktelow, N. S. (1985), The Simplon line: A major displacement zone in the western Lepontine Alps, *Eclogae Geol. Helv.*, *78*, 73–96.

Marshall, D., N. Meisser, and R. P. Taylor (1998a), Fluid inclusion, stable isotope and Ar-Ar evidence for the age and origin of gold-bearing quartz veins at Mont Chemin, Switzerland, *Mineral. Petrol.*, *62*, 147–165.

Marshall, D., H.-R. Pfeifer, J. C. Hunziker, and D. L. Kirschner (1998b), A pressure-temperature path for the NE Mont-Blanc massif: Fluid-inclusion, isotopic and thermobarometric evidence, *Eur. J. Mineral.*, *10*, 1227–1240.

Masson, H., R. Herb, and A. Steck (1980), Helvetic Alps of western Switzerland, in *Geology of Switzerland: A Guide Book (Part B)*, edited by R. Trümpy, pp. 109–153, Wepf and Co., Basel.

Mulch, A., and M. A. Cosca (2004), Recrystallization or cooling ages: In situ UV-laser $^{40}Ar/^{39}Ar$ geochronology of muscovite in mylonitic rocks, *J. Geol. Soc.*, *161*(4), 573–582.

Müller, W., D. Aerden, and A. N. Halliday (2000a), Isotopic dating of strain fringe increments: Duration and rates of deformation in shear zones, *Science*, *288*(5474), 2195–2198.

Müller, W., N. S. Mancktelow, and M. Meier (2000b), Rb-Sr microchrons of synkinematic mica in mylonites: An example from the DAV fault of the Eastern Alps, *Earth Planet. Sci. Lett.*, *180*(3–4), 385–397.

Platt, J. P. (1984), Balanced cross-sections and their implications for the deep structure of the northwest Alps: Discussion, *J. Struct. Geol.*, *6*(5), 603–606.

Poty, B., H. A. Stalder, and A. M. Weisbrod (1974), Fluid inclusions studies in quartz from fissures of Western and central Alps, *Schweiz. Mineral. Petrogr. Mitt.*, *54*, 717–752.

Ramsay, J. G. (1989), Fold and fault geometry in the western Helvetic nappes of Switzerland and France and its implications for the evolution of the arc of the Western Alps, in *Alpine Tectonics*, edited by M. Coward and D. Dietrich, *Geol. Soc. Spec. Publ.*, 33–45.

Ramsay, J. G., M. Casey, and R. Kligfield (1983), Role of shear in development of the Helvetic fold-thrust belt of Switzerland, *Geology*, *11*(8), 439–442.

Reddy, S. M., and G. J. Potts (1999), Constraining absolute deformation ages: The relationship between deformation mechanisms and isotope systematics, *J. Struct. Geol.*, *21*(8–9), 1255–1265.

Reinhard, M., and H. Preiswerk (1927), Ober Granitmylonite im Aiguilles-Rouges-Massiv (Westliches Wallis), *Verh. Naturforsch. Ges. Basel*, *38*, 188–200.

Renne, P. R., C. C. Swisher, A. L. Deino, D. B. Karner, T. L. Owens, and D. J. DePaolo (1998), Intercalibration of standards, absolute ages and uncertainties in $^{40}Ar/^{39}Ar$ dating, *Chem. Geol.*, *145*(1–2), 117–152.

Rolland, Y., S. Cox, A. M. Boullier, G. Pennacchioni, and N. S. Mancktelow (2003), Rare earth and trace element mobility in mid-crustal shear zones: Insights from the Mont Blanc massif (Western Alps), *Earth Planet. Sci. Lett.*, *214*(1–2), 203–219.

Rolland, Y., M. Corsini, M. Rossi, S. F. Cox, G. Pennacchioni, N. S. Mancktelow, and A. M. Boullier (2007), Comment on "Alpine thermal and structural evolution of the highest external crystalline massif: The Mont Blanc" by P. H. Leloup, N. Arnaud, E. R. Sobel, and R. Lacassin, *Tectonics*, *26*, TC2015, doi:10.1029/2006TC001956.

Rolland, Y., M. Rossi, S. F. Cox, M. Corsini, N. S. Mancktelow, G. Pennacchioni, M. Fornari, and A. M. Boullier (2008), $^{40}Ar/^{39}Ar$ dating of synkinematic white mica: Insights from fluid-rock reaction in low-grade shear zones (Mont Blanc massif) and constraints on timing of deformation in the NW external Alps, *Geol. Soc. London, Spec. Publ.*, *299*(1), 293–315.

Rossi, M., and Y. Rolland (2014), Stable isotope and Ar/Ar evidence of prolonged multiscale fluid flow during exhumation of orogenic crust: Example from the Mont Blanc and Aar massifs (NW Alps), *Tectonics*, *33*, 1681–1709, doi:10.1002/2013TC003438.

Rossi, M., Y. Rolland, O. Vidal, and S. F. Cox (2005), Geochemical variations and element transfer during shear-zone development and related episyenites at middle crust depths: Insights from the Mont Blanc granite (French-Italian Alps), *Geol. Soc. London, Spec. Publ.*, *245*(1), 373–396.

Seward, D., and N. S. Mancktelow (1994), Neogene kinematics of the central and Western Alps: Evidence from fission-track dating, *Geology*, *22*, 803–806.

Simon-Labric, T., Y. Rolland, T. Dumont, T. Heymes, C. Authemayou, M. Corsini, and M. Fornari (2009), $^{40}Ar/^{39}Ar$ dating of Penninic front tectonic displacement (W Alps) during the lower Oligocene (31–34 Ma), *Terra Nova*, *21*(2), 127–136.

Soom, M. (1990), Abkühlungs- und Hebungsgeschichte der Externmassive und der penninischen Decken beidseits der Simplon-Rhone-Linie seit dem Oligozän: Spaltspurdatierungen an Apatit/Zirkon und K-Ar-Datierungen an Biotit/Muskowit (Westliche Zentralalpen), PhD thesis, Univ. Bern, Bern, Switzerland.

Steck, A., and J. Hunziker (1994), The Tertiary structural and thermal evolution of the central Alps—Compressional and extensional structures in an orogenic belt, *Tectonophysics*, *238*(1–4), 229–254.

Steck, A., and D. Vocat (1973), Zur Mineralogie der Granitmylonite von Mieville, Aiguilles-Rouges-Massiv, *Schweiz. Mineral. Petrogr. Mitt.*, *53*(3), 474–477.

Steck, A., J. L. Epard, A. Escher, P. Lehner, R. Marchant, and H. Masson (1997), Geological interpretation of the seismic profiles through western Switzerland: Rawil (W1), Val d'Anniviers (W2), Mattertal (W3), Zmutt-Zermatt-Findelen (W4) and Val de Bagnes (W5), in *Deep Structure of the Swiss Alps—Results From NRP 20*, edited by O. A. Pfiffner et al., pp. 123–137, Birkhäuser, Basel, Switzerland.

Steck, A., J.-L. Epard, A. Escher, Y. Gouffon, and H. Masson (2001), Notice explicative pour la carte tectonique des Alpes de Suisse occidentale, *Swisstopo*, 73 pp., Bern, Switzerland.

Steiger, R. H., and E. Jäger (1977), Subcommission on geochronology: Convention on the use of decay constants in geo- and cosmochronology, *Earth Planet. Sci. Lett.*, *36*(3), 359–362.

Trümpy, R. (1980), *Geology of Switzerland: A Guide Book. Part A: An Outline of the Geology of Switzerland*, 104 pp., Wepf & Co., Basel.

Valla, P. G., P. A. van der Beek, D. L. Shuster, J. Braun, F. Herman, L. Tassan-Got, and C. Gautheron (2012), Late Neogene exhumation and relief development of the Aar and Aiguilles Rouges massifs (Swiss Alps) from low-temperature thermochronology modeling and $^{4}He/^{3}He$ thermochronometry, *J. Geophys. Res.*, *117*, F01004, doi:10.1029/2011JF002043.

Vernon, A. J., P. A. van der Beek, H. D. Sinclair, and M. K. Rahn (2008), Increase in late Neogene denudation of the European Alps confirmed by analysis of a fission-track thermochronology database, *Earth Planet. Sci. Lett.*, *270*(3–4), 316–329.

Villa, I. (1998), Isotopic closure, *Terra Nova*, *10*(1), 42–47.

von Raumer, J. F. (1971), Das Mont-Blanc-Massiv: Altkristallin im Bereich schwacher alpiner Metamorphose, *Schweiz. Mineral. Petrogr. Mitt.*, *51*, 193–225.

von Raumer, J. F. (1974), Zur Metamorphose amphibolitischer Gesteine im Altkristallin des Mont-Blanc- und Aiguilles-Rouges-Massivs, *Schweiz. Mineral. Petrogr. Mitt.*, *54*, 471–488.

von Raumer, J. F., and F. Bussy (2004), Mont Blanc and Aiguilles Rouges; Geology of their polymetamorphic basement (external massifs, Western Alps, France-Switzerland), *Mém. Géol. (Lausanne)*, *42*, 302.

West, D. P., and D. R. Lux (1993), Dating mylonitic deformation by the 40Ar-39Ar method: An example from the Norumbega fault zone, Maine, *Earth Planet. Sci. Lett.*, *120*(3–4), 221–237.